Stochastic uncertainty of advected curves in finite-time unsteady flows

Sanjeeva Balasuriya
School of Mathematical Sciences, University of Adelaide, Adelaide SA 5005, Australia
(Received 21 March 2017; published 2 June 2017)

Identifying coherent structures in unsteady flows acting over a finite-time is a well-established research area, in part due to the applicability to realistic velocities obtained from experimental, observational, or numerically generated data. More recently, there is an emerging need to understand the impact of small-scale uncertainties on larger scale structures; for example, the "stochastic parametrization" problem in climate models. This article establishes a rigorous tool in this direction, specifically quantifying the uncertainty of advected curves in the presence of small stochasticity. Explicit expressions are derived for the expectation and the variance of the curves' location. The velocity field may be unsteady and compressible, and the Wiener process driving the stochasticity can have general spatiotemporal dependence. Monte Carlo simulations are used to verify the uncertainty expressions.

DOI: 10.1103/PhysRevE.95.062201

I. INTRODUCTION

There has recently been considerable interest in evaluating the impact on trajectories when an unsteady velocity field operates over a finite time interval. The motivation for this is the fact that in all realistic velocity fields obtained from experiments (using particle image velocimetry, say) or observations (from oceanic measurements, for example), data is explicitly available only over a finite time [1]. In many such cases, there is a need to determine (time-varying) transport or transport barriers [1–4]. Essentially, all methods that have been developed in this sense use the velocity data as *deterministic*. However, in all realistic cases, there is some uncertainty in the velocity measurements [5–7]. This may be modeled using stochasticity, and there are methods which address issues such as quantifying the resulting decorrelation [8,9], decoding the stochasticity from observations [5,10], determining an effective diffusivity [11–14], or obtaining properties of mean derivatives [15]. This article is concerned with a different aspect of such uncertainties: given a stochastic model for the uncertainty in a two-dimensional unsteady velocity field, is it possible to quantify the uncertainty of an advected curve?

Here, the two-dimensional advection is formulated in terms of a stochastic differential equation, with the stochasticity formed from a Wiener process, which is modulated by a (potentially spatially and temporally dependent) diffusion matrix. Numerical simulations of a particular curve of initial conditions would result in stochastic trajectories, which are scattered around the deterministically advected curve. The curve therefore acquires an uncertainty, and this article first determines the expected location of the stochastically advected curve at later times. Unsurprisingly, this is to leading-order exactly the deterministically advected curve. Second, the focus is on quantifying the uncertainty. This is defined in terms of the square-root of the variance of the scattered trajectories in the normal direction to the deterministically advected curve. An expression for this width, valid in the limit of small stochasticity, is obtained with the help of Itô's lemma and Itô's isometry [16,17]. This enables the definition of a widening zone around the deterministically advected curve in which realizations of stochastic advection are most likely to lie.

This article is organized as follows. Section II explains the theoretical approach for computing the curve's uncertainty. Implications to elementary flows and Taylor dispersion is briefly presented in Sec. III. Section IV applies the theory to the flow of the forced Duffing equation and validates the uncertainty expressions, as well as their errors, quantitatively in relation to Monte Carlo simulations. An anisotropic spatially varying diffusion matrix is used in these computations. Section V uses a compressible flow model and examines an isotropic diffusion matrix—including one which has time-variation—and performs analogous validations of the theory. Section VI discusses future and ongoing directions. Appendix A provides the proof of the uncertainty expressions presented in Sec. II, and Appendix B provides additional details on the time-validity and simplifications of those results.

II. STOCHASTIC CURVE UNCERTAINTY

Consider the finite-time unsteady deterministic flow,

$$\dot{\boldsymbol{x}} = \boldsymbol{u}(\boldsymbol{x},t), \tag{1}$$

where $x \in \Omega$ is two-dimensional, and Eq. (2) is only defined during the finite-time interval $t \in [t_1,t_2]$. It is possible that $\boldsymbol{u}$ is known only via data, obtained from experiments or observations, or alternatively from the output of a direct numerical simulation. Suppose $\mathcal{C}(t_1)$ is a simple smooth curve chosen as an initial condition to Eq. (1), and when materially advected generates the curve $\mathcal{C}(t)$ for $t \in [t_1,t_2]$. The intuitive question addressed is: is it possible to quantify the uncertainty in $\mathcal{C}(t)$ when a stochastic perturbation is included in Eq. (1)?

To address this, first Eq. (1) will be written in the stochastic differential equations notation as

$$d\boldsymbol{x}_t = \boldsymbol{u}(\boldsymbol{x}_t,t)dt. \tag{2}$$

The stochastic perturbation to this will be represented in the standard form [18] by

$$d\boldsymbol{y}_t = \boldsymbol{u}(\boldsymbol{y}_t,t)dt + \varepsilon\sigma(\boldsymbol{y}_t,t)d\boldsymbol{W}_t \quad t \in [t_1,t_2], \tag{3}$$

for $\boldsymbol{y}_t \in \Omega$, in which $d\boldsymbol{W}_t$ represents a two-dimensional Wiener process, $0 < \varepsilon \ll 1$ and σ is a bounded and suitably smooth 2×2 matrix representing diffusion. Thus, $\boldsymbol{y}_t$ is a random process in contrast to $\boldsymbol{x}_t$. The presence of both spatial and temporal dependence in each of the four components of σ allows for spatiotemporal anisotropy and heterogeneity of

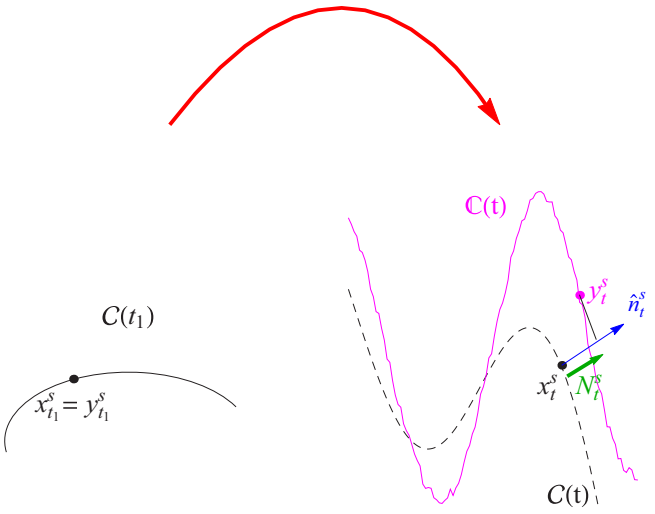

FIG. 1. The advection of $\mathcal{C}(t_1)$ from the time t_1 (left) to the time t (right), showing the resulting deterministic curve $\mathcal{C}(t)$ (dashed black) and a stochastic realization $\mathfrak{C}(t)$ (solid magenta).

the diffusion process. If $\mathcal{C}(t_1)$ is chosen as an initial condition for Eq. (3), and evolves into the time-varying curve $\mathfrak{C}(t)$, the issue is to characterize the random and nondifferentiable $\mathfrak{C}(t)$ in comparison to the deterministic $\mathcal{C}(t)$.

The definitions to follow are pictured in Fig. 1. Parametrize $\mathcal{C}(t_1)$ by s in the form $\boldsymbol{x}^s_{t_1}$, where $\boldsymbol{x}^s_t$ for each s would solve Eq. (2). Differentiability of $\boldsymbol{x}^s_t$ in s is guaranteed by the smoothness assumption on $\mathcal{C}(t_1)$. Let $\boldsymbol{y}^s_t$ be the solution to Eq. (3) under identical initial conditions, that is, $\boldsymbol{y}^s_{t_1} = \boldsymbol{x}^s_{t_1}$ for all s. Define for vectors $\boldsymbol{f} = (f_1, f_2) \in \mathbb{R}^2$, the perpendicular vector $\boldsymbol{f}^\perp := (-f_2, f_1)$ obtained by rotating $\boldsymbol{f}$ by $+\pi/2$. The *random normal displacement* N^s_t will be defined by

$$N^s_t := \left[\boldsymbol{y}^s_t - \boldsymbol{x}^s_t\right] \cdot \hat{\boldsymbol{n}}^s_t \quad , \quad \text{for} \quad t \in [t_1, t_2], \tag{4}$$

where

$$\hat{\boldsymbol{n}}^s_t := \left(\frac{\partial \boldsymbol{x}^s_t}{\partial s}\right)^\perp \Big/ \left|\frac{\partial \boldsymbol{x}^s_t}{\partial s}\right| \tag{5}$$

gives a unit normal vector to $\mathcal{C}(t)$ at the location $\boldsymbol{x}^s_t$. This N^s_t characterizes the normal displacement of $\mathfrak{C}(t)$ in comparison to $\mathcal{C}(t)$ at each $t \in [t_1, t_2]$. If thinking in terms of explicitly the impact of the full finite time inverval $[t_1, t_2]$, understanding $N^s_{t_2}$ may be the goal. However, more generality will be pursued here, in the sense of understanding the *evolution* of N^s_t until time t_2.

Under the conditions that the second-order spatial derivatives of $\boldsymbol{u}$ and the first-order spatial derivatives of σ are bounded, it is shown in Appendix A that, correct to $O(\varepsilon)$,

$$N^s_t = \frac{\varepsilon \int_{t_1}^t e^{\int_\xi^t [\nabla \cdot \boldsymbol{u}](\boldsymbol{x}^s_\eta, \eta) d\eta} \left(\left[\frac{\partial \boldsymbol{x}^s_\xi}{\partial s}\right]^\perp\right)^\top \sigma\left(\boldsymbol{x}^s_\xi, \xi\right) d\boldsymbol{W}_\xi}{\left|\frac{\partial \boldsymbol{x}^s_t}{\partial s}\right|}, \tag{6}$$

where $(\boldsymbol{.})^\top$ is the transpose. The proof uses an application of Itô's lemma for a certain Itô process associated with the stochastic differential Eq. (3). Equation (6) tells us of the distribution of the random curves $\mathfrak{C}(t)$ when considered in the normal direction to $\mathcal{C}(t)$ from a point $\boldsymbol{x}^s_t$ on it. Given the fact that all the terms in the integrand above are deterministic, standard stochastic calculus results [16,17] give the fact that the expectation of the normal displacement is

$$E\left[N^s_t\right] = 0 \tag{7}$$

to $O(\varepsilon)$ for all s. This gives the unsurprising fact that, on average, $\mathfrak{C}(t)$ will exhibit no movement in the normal direction from $\mathcal{C}(t)$. Next, the square-root of the variance of N^s_t will provide an estimate of a width around $\mathcal{C}(t)$ in which $\mathfrak{C}(t)$ lies. Now, since the expectation is zero to leading order,

$$\begin{aligned} w^s_t &:= \sqrt{\mathrm{Var}\left[N^s_t\right]} \\ &= \frac{\varepsilon}{\left|\frac{\partial \boldsymbol{x}^s_t}{\partial s}\right|} \sqrt{E\left[\left(\int_{t_1}^t e^{\int_\xi^t [\nabla \cdot \boldsymbol{u}](\boldsymbol{x}^s_\eta, \eta) d\eta} \left(\left[\frac{\partial \boldsymbol{x}^s_\xi}{\partial s}\right]^\perp\right)^\top \sigma\left(\boldsymbol{x}^s_\xi, \xi\right) d\boldsymbol{W}_\xi\right)^2\right]}. \end{aligned} \tag{8}$$

By a straightforward application of Itô's isometry [16,17] to the stochastic integral above, this width estimate is given by

$$w^s_t = \frac{\varepsilon \left(\int_{t_1}^t e^{2\int_\xi^t [\nabla \cdot \boldsymbol{u}](\boldsymbol{x}^s_\eta, \eta) d\eta} \left|\sigma^\top \left(\boldsymbol{x}^s_\xi, \xi\right) \left(\frac{\partial \boldsymbol{x}^s_\xi}{\partial s}\right)^\perp\right|^2 d\xi\right)^{1/2}}{\left|\frac{\partial \boldsymbol{x}^s_t}{\partial s}\right|}. \tag{9}$$

This is the expression for the expected uncertainty in the *width* of the stochastically advected curve. (The curve $\mathfrak{C}(t)$ also acquires a *tangential displacement* along $\mathcal{C}(t)$ in general, which can if necessary be determined using the determinisitc ideas in Ref. [19]. However, the formulas will be unwieldy, and moreover the fact that tangentially moving a curve has little visible effect means that this motion can be ignored for our purposes.) The t is time, and the s-variable represents the location $\boldsymbol{x}^s_t$ at which the normal is drawn to $\mathcal{C}(t)$.

It will be reiterated that both Eqs. (6) and (9) should also include additive $O(\varepsilon^2)$ terms, which will be omitted for brevity throughout the main text of this article. Since the expression in Eq. (9) contains only the $O(\varepsilon)$ term, a legitimate question would be whether there are time restriction imposed by ignoring the higher-order terms. It is shown in Appendix B that the time-interval of validity of the first-order expression in Eq. (9) obeys $t - t_1 \sim \varepsilon^{-2}$, as long as the deterministic curve does not acquire strong folds during the time-interval $[t_1, t]$, which could lead to abruptness in the variation of $\hat{\boldsymbol{n}}^s_t$.

The width expression Eq. (9) allows for defining a region

$$R_\alpha(t) := \bigcup_s \bigcup_{r \in [-\alpha w^s_t, +\alpha w^s_t]} \left\{\boldsymbol{x}^s_t + r\, \hat{\boldsymbol{n}}^s_t\right\}, \tag{10}$$

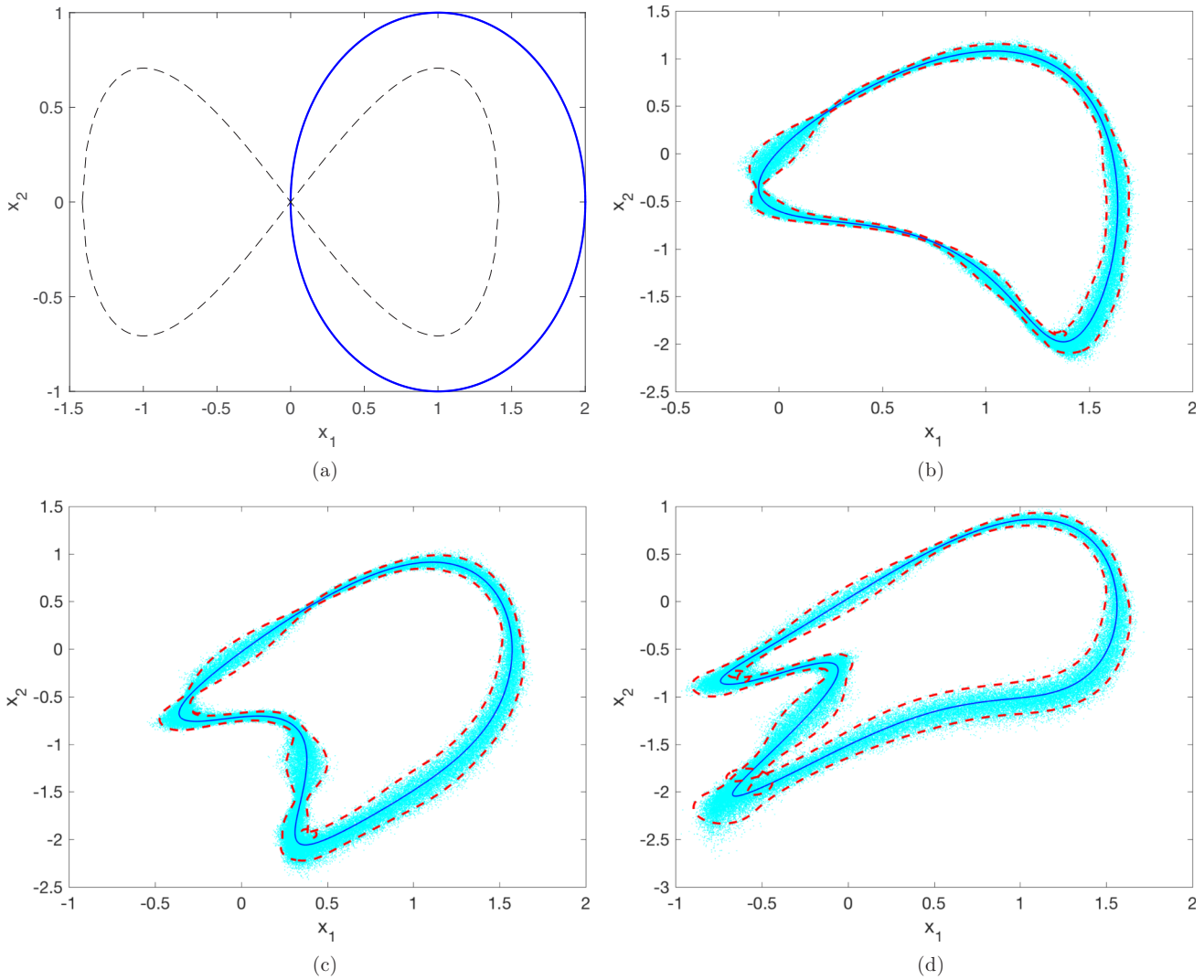

FIG. 2. Original curve (a), and subsequent advected curve points (cyan), with the deterministically advected curve (solid blue) and the theoretical $R_2(t)$ (red dashed), for the stochastic Duffing equation as described in Sec. IV: (b) $t = 0.5$, (c) $t = 1$, and (d) $t = 1.5$.

in which $\mathfrak{C}(t)$ is more likely to be. Here, α is a factor indicating how many widths w_t^s away from the deterministically advected curve the region is defined. Thus, $R_\alpha(t)$ may be thought of as a "widening zone" of the curve $\mathcal{C}(t)$ due to stochastic uncertainty. Since Eq. (9) represents a standard deviation, a sensible value for α might be 2 (in line with the fact that a Gaussian distribution has 95% of its data within two standard deviations). So $R_2(t)$ might be considered a *heuristic* [20] "95% confidence interval" region around $\mathcal{C}(t)$.

The quantities $N_{t_2}^s$, $w_{t_2}^s$, and $R_\alpha(t_2)$ would be relevant to commonly studied *fixed*-step finite-time methods only interested in the impact at a fixed final time t_2. In contrast, the general expressions here catalog the *time-variation* during the interval $[t_1,t_2]$ as an added benefit.

III. ELEMENTARY FLOWS

Before using the width Eq. (9) in its generality, a situation in which it provides a highly simplified formula will be considered and related to intuition from elementary flows. Appendix B details the simplifications to Eqs. (9) and (6), which occur in two highly pertinent situations: the fluid being incompressible ($\nabla \cdot u = 0$), and/or the diffusion being isotropic and constant ($\sigma = \mathrm{Id}$). While the reader is referred to Appendix B for details, the simplification to Eq. (9) under *both* incompressibility and isotropic constant diffusion will be stated here:

$$w_t^s = \varepsilon \left(\int_{t_1}^{t} \left(T_{\xi;t}^s \right)^2 d\xi \right)^{1/2}, \tag{11}$$

where the *relative local tangential expansion* associated with the determinstic flow is given by

$$T_{\xi;t}^s := \left| \frac{\partial \boldsymbol{x}_\xi^s}{\partial s} \right| \Big/ \left| \frac{\partial \boldsymbol{x}_t^s}{\partial s} \right|, \quad \xi \in [t_1,t]. \tag{12}$$

The word "relative" here means relative to the *final* time t.

The first observation from Eq. (11) is that if the flow were still (i.e., $\boldsymbol{u} \equiv \boldsymbol{0}$), then $T_{\xi;t}^s = 1$, and so $w_t^s = \varepsilon\sqrt{t - t_1}$ irrespective of the point on the curve, or the nature of the curve, chosen. This is, of course, the classical expectation for two-dimensional Brownian motion. In a more general flow,

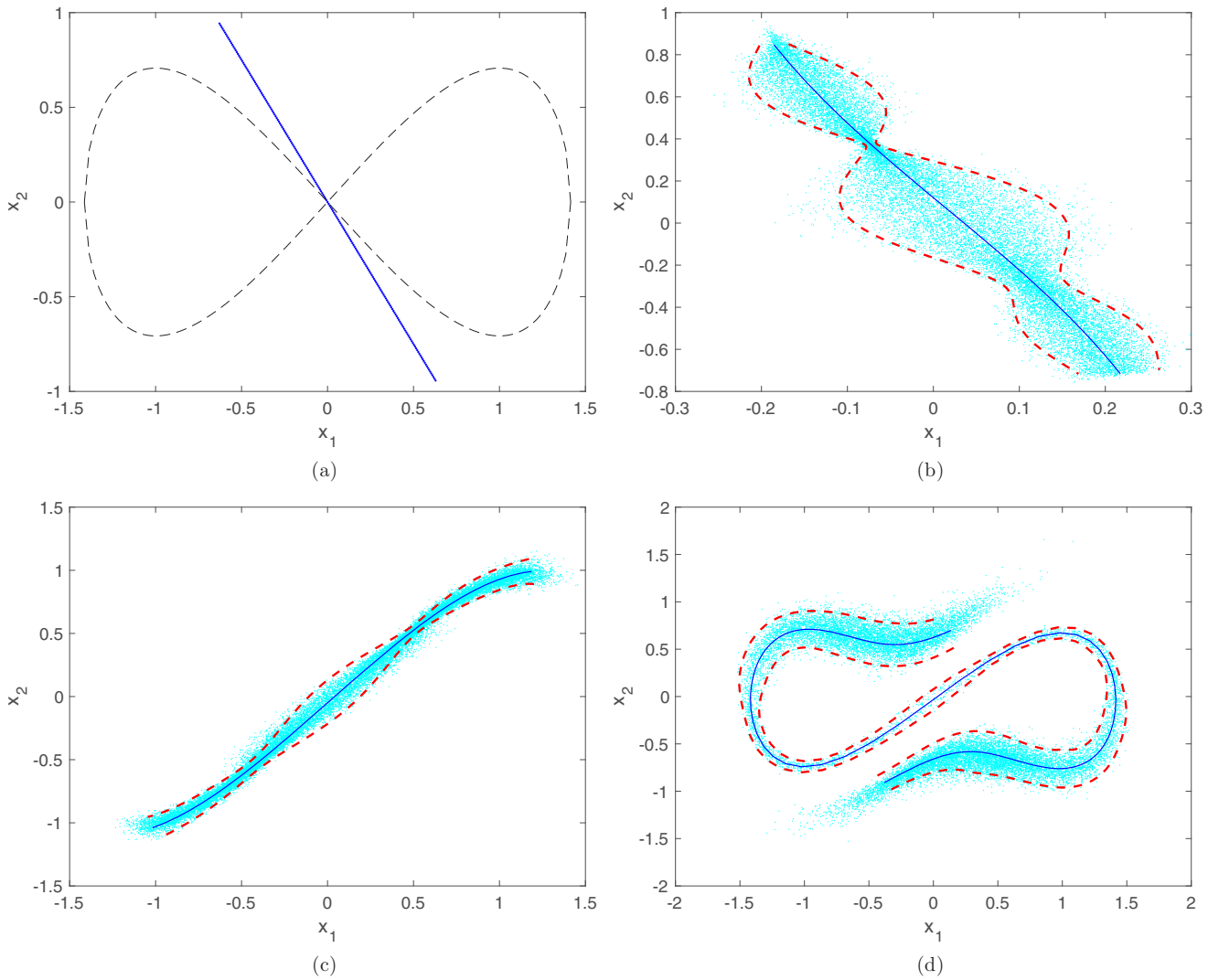

FIG. 3. Original curve (a), and subsequent advected curve points (cyan), with the deterministically advected curve (solid blue) and $R_2(t)$ (dashed red), for the stochastic Duffing equation as described in Sec. IV: (b) $t = 0.5$, (c) $t = 2$, and (d) $t = 5$.

Eq. (11) indicates that the width is ε times the L^2-norm of the expansion rate $T^s_{\xi;t}$. Thus, the resulting width occurs as an interaction between the stretching rate and Brownian motion.

To elucidate this further, consider a steady extensional flow that has a stretching rate of $\lambda > 0$ in a certain direction, and suppose $\mathcal{C}(t_1)$ is a line that lies along the direction of stretching. Then, from Eq. (11),

$$w^s_t = \varepsilon\left(\int_{t_1}^{t}\left(\frac{e^{\lambda\xi}}{e^{\lambda t}}\right)^2 d\xi\right)^{1/2} = \varepsilon\left(\frac{1-e^{2\lambda(t_1-t)}}{2\lambda}\right)^{1/2}. \quad (13)$$

For small $t - t_1$, $w^s_t \sim \varepsilon\sqrt{t-t_1}$ independent of λ, and for large t, this asymptotes to the constant value $\varepsilon/\sqrt{2\lambda}$. The small $t - t_1$ limit is exactly what is expected of the standard deviation of the absolute dispersion in hyperbolic flow regions [21–23], and the long-time constant value represents the limiting situation in which the diffusion balances the stretching. In contrast, if $\mathcal{C}(t_1)$ were taken to be a straight line *normal* to the direction of stretching, the width expansion for all times would be given by the Brownian form $w^s_t = \varepsilon\sqrt{t-t_1}$, which does not approach a constant.

For the more general width expression, Eq. (9), the interaction between the stretching rate and the diffusion is more complex, and its impact will be assessed in two more examples.

IV. DUFFING OSCILLATOR

The first numerical validation of the results will be performed using the standard Duffing oscillator model [24],

$$\begin{aligned}\dot{x}_1 &= x_2\\ \dot{x}_2 &= x_1 - x_1^3 + 0.2\sin(2\pi t)\end{aligned}, \quad (14)$$

in which particular choices have been made for the parameters in the time-periodic forcing, as the unsteady flow Eq. (2). For the corresponding stochastic differential Eq. (3), take

$$\sigma(x_1,x_2,t) = \begin{pmatrix} 1+3\cos(5x_2) & \sin(\pi x_1)\\ \left(x_1-\frac{3}{2}\right)x_2^2 & e^{x_2}\end{pmatrix}, \quad (15)$$

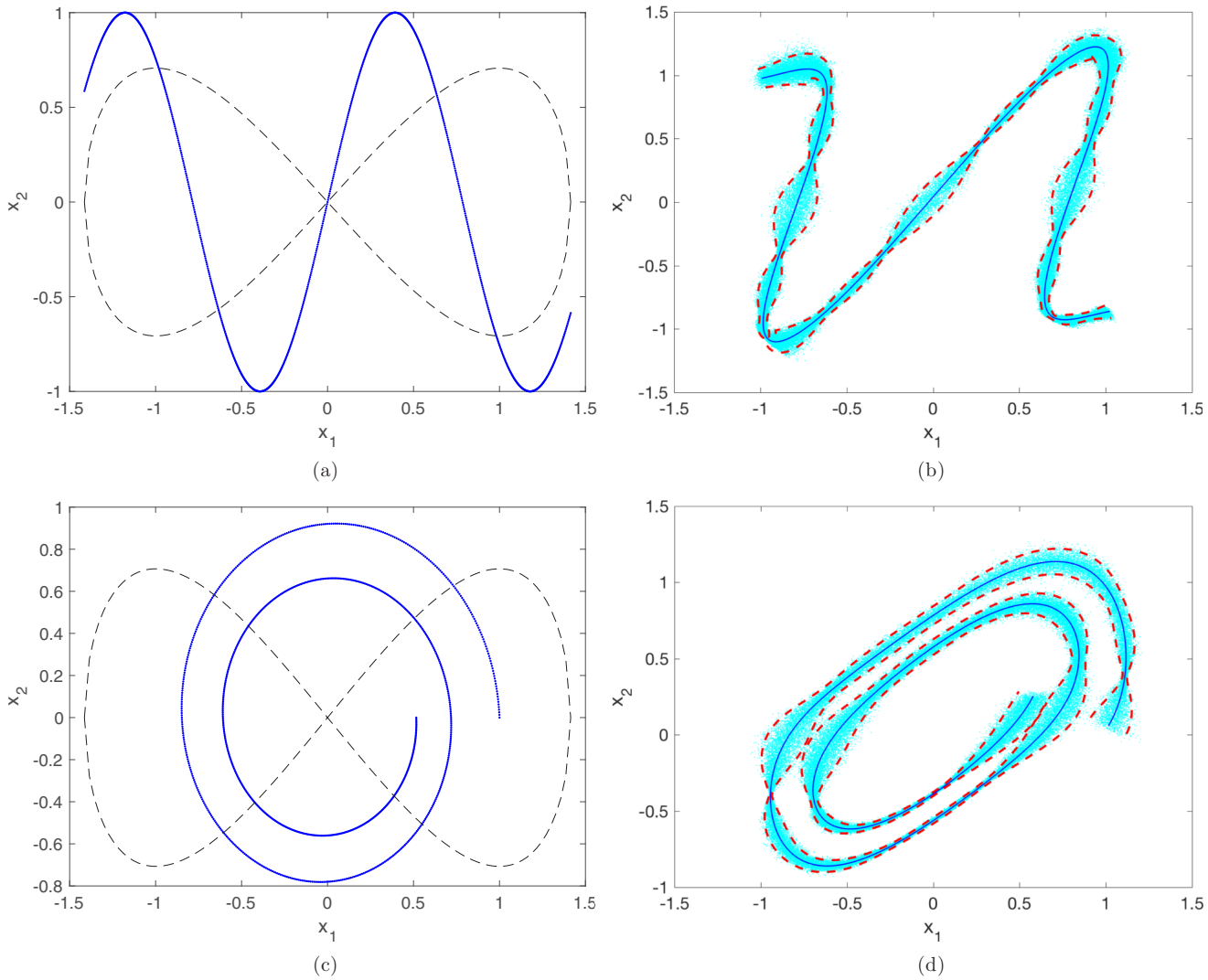

FIG. 4. Several choices of initial curves seeded with 1000 points [left panel], and their resulting stochastic advection [right panel] under the Duffing flow to time $t = 0.5$.

which is inhomogeneous across the domain. Different parts of an advected curve will therefore experience different diffusion depending on where they are located at each time instance of advection. Throughout this example, the initial time is $t_1 = 0$, and $\varepsilon = 0.02$ is chosen. In numerically advecting the stochastic differential Eq. (3), the Euler-Maruyama scheme [25] is used. To maintain the fact that the stochasticity is considered small in comparison to the base flow Eq. (14), it is necessary to have $|\varepsilon| \ll \sqrt{\Delta t}$, where Δt is the time-step used in the Euler-Maruyama scheme. Consequently, the choice $\Delta t = 0.01$ is made.

For the first numerical experiment, the closed circular blue curve as shown in Fig. 2(a) is considered. This is seeded with 1000 points, and each point is advected under the stochastic differential Eq. (3) with σ given by Eq. (15). The dashed curve shown in Fig. 2(a) is the heteroclinic loop of the Duffing system in the absence of forcing; the forced system Eq. (14) has chaotic bands occurring nearby these dashed curves. The points on the blue curve were advected using the Euler-Maruyama scheme to generate 1000 points at the time t, thereby obtaining points along one realization of the curve $\mathfrak{C}(t)$. The 10^5 points resulting from performing 100 such simulations are shown collectively in the other subfigures of Fig. 2, at different final times t, as cyan dots. The solid blue curve in each figure is the deterministically advected curve, whereas the cyan dots scatter around it. The dashed red boundary drawn around this was computed using Eq. (9) and identifies $R_2(t)$ (i.e., the heuristic for the 95% confidence interval). In this case, the velocity field Eq. (14) is area-preserving, and thus the term $\nabla \cdot \boldsymbol{u} = 0$, leading to simplifications in Eq. (9). In performing this computation, it was necessary to keep track of the deterministically advected curve, and also compute the derivative of the curve location with respect to the parameter s. This was accomplished by thinking of s, which parametrizes the blue curve in Fig. 2(a) as simply being an index assigned to each point (so $s \in \{1,2,\ldots,1000\}$ in this instance). Then, at any subsequent time ξ, the quantity $\partial \boldsymbol{x}_\xi^s / \partial s$ could be numerically approximated by $\boldsymbol{x}_\xi^{s+1} - \boldsymbol{x}_\xi^s$, and inserted into Eq. (9).

In Figs. 2(b) and 2(c), the simulations show regions where there is large scattering from the deterministic curve and other regions where the normal dispersion is small. The theoretical

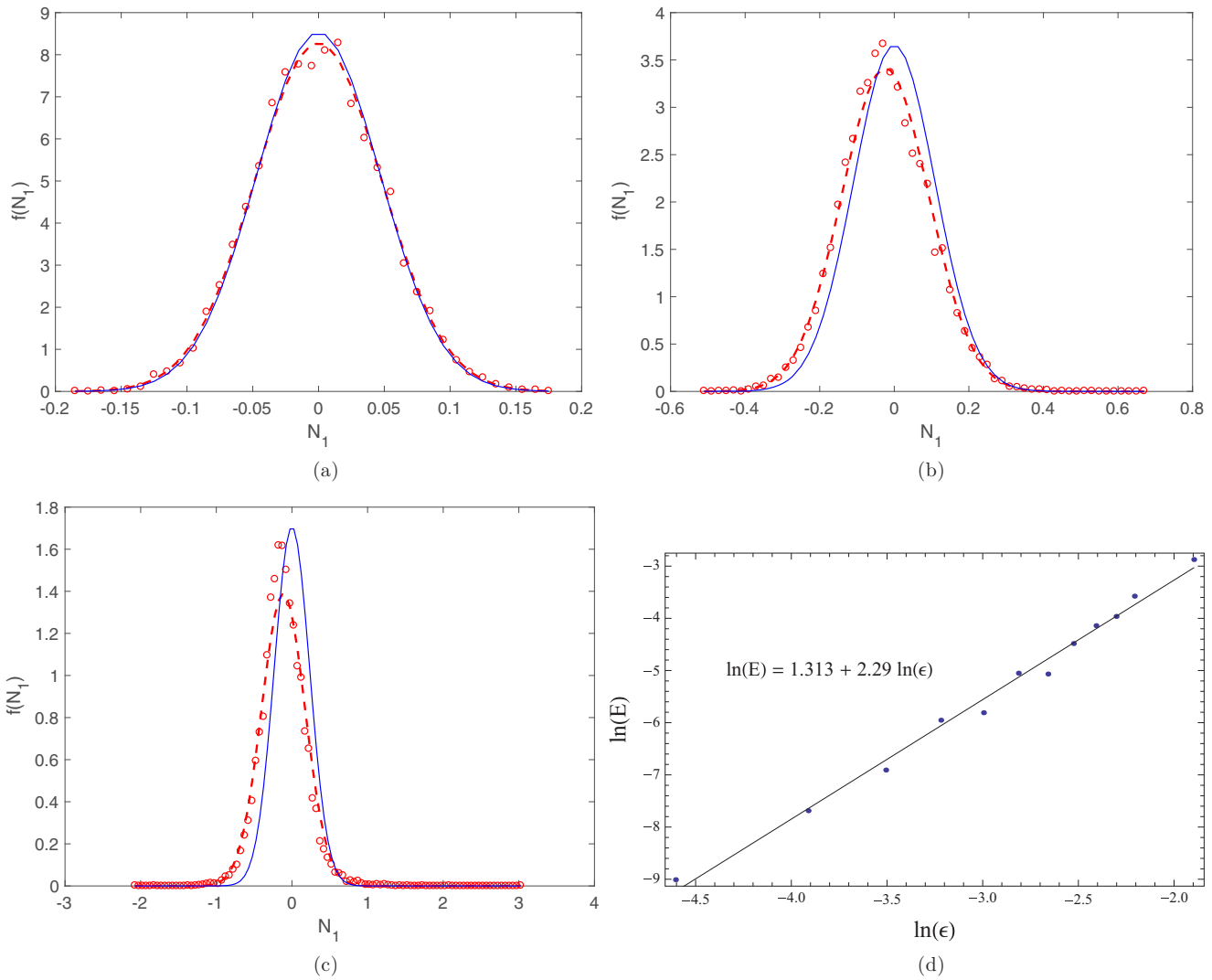

FIG. 5. A comparison between the frequency statistics $f(N_1)$ of the numerically simulated N_1 (red circles), its imputed normal distribution (dashed red curve), and theoretical (normalized) distribution (solid blue curve) for (a) $\varepsilon = 0.03$, (b) $\varepsilon = 0.07$, and (c) $\varepsilon = 0.15$ for the Duffing flow as described in the text. (d) Variation of the error Eq. (16) with ε (blue dots) and a linear fit.

(red-dashed) region does an excellent job of capturing this varying stochastic width along the curve. The regions in which there are bulges, and regions in which the stochastic simulations are mostly pinched toward the blue deterministic curve, are well approximated. By Fig. 2(d), the R_2 still delineates the scatter quite well, but some difficulties have emerged, which illustrates why R_α cannot be rigorously thought of as an envelope in general. The reason for this is that there are several points at which the deterministic curve has large curvature, and hence the normal vector to this curve—the direction in which the stochastic width is computed in Eq. (9)—undergoes a sharp transition. Basically, if the local osculating circle has radius of the order of ε or smaller, Eq. (10) with $r = \pm\alpha w_t^s$, with the sign chosen such that one is going in the direction of the osculating circle, can lead to multivaluedness. Intuitively, these difficulties arise when the curve folds unduly. This is certainly the expectation when curve points pass through the chaotic zone, which leads to the stretching and folding behavior whose inception is visible in Fig. 2(d). If the curve has significantly folded, of course, expressing a stochastic widening zone makes less sense.

Tests were also performed by seeding many more points ($\sim 10^5$). The scattered points filled in the $R_2(t)$ in an even more conclusive fashion than in Fig. 2, respecting the thicker and thinner regions. (These are not shown here because of the size of the figure files becomes unwieldy.)

Next, the alternative initial curve as shown in Fig. 3(a) is considered. As chosen, this is almost tangential to the stable manifold at the origin. As time progresses, the advected deterministic curve is expected to approach the unstable manifold of the hyperbolic trajectory of Eq. (14) that moves around in a periodic fashion near the origin. The solid blue curves (again with 100 simulations) in Figs. 3(b)–3(d) illustrate the time-evolution of this approach. By $t = 0.5$, the deterministic curve shortens, but the stochastic expansion in the normal direction is large because the unstable manifold's attraction is roughly in the same direction. As time progresses, the curve gets pulled along the unstable manifold. Once again, the shape of $R_2(t)$ captures the thickness of the stochastic

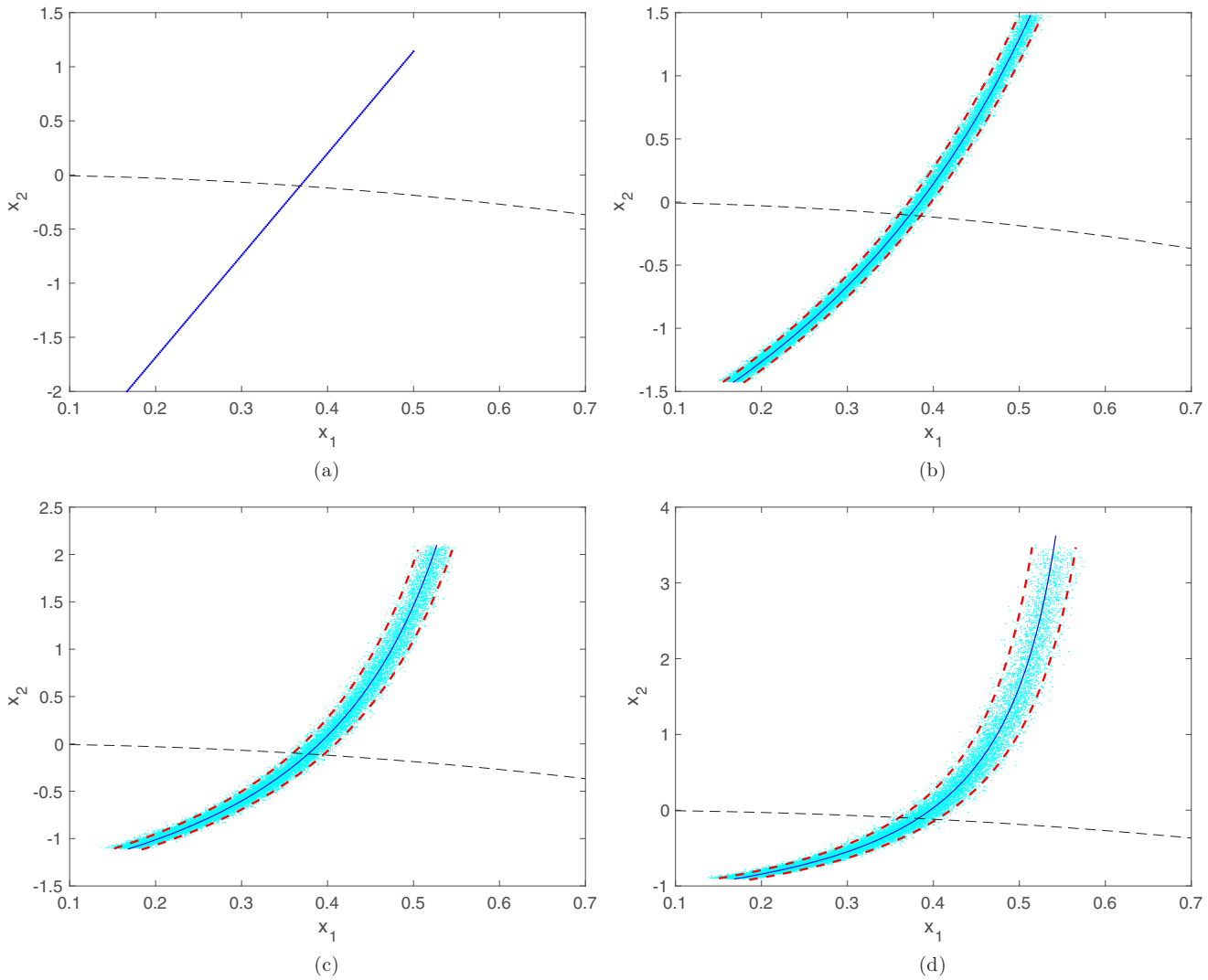

FIG. 6. Original curve (a), and subsequent advected curve points (cyan), with the deterministically advected curve (solid blue) and the theoretical zone $R_2(t)$ (dashed red), for the flow Eq. (17) stochastically perturbed with $\sigma = \mathrm{Id}$. The flow Eq. (17) is expanding above the dashed black curve. (b) $t = 0.1$, (c) $t = 0.2$, and (d) $t = 0.3$.

widening displayed by the simulations. Notice, however, that the number of numerical iterates near the origin is very small by $t = 5$; this is since the unstable manifold pulls iterates out at an exponential rate. While not populated by sufficiently many simulations to enable a comparison in Fig. 3(d), a theoretical width assessment in the vicinity of this hyperbolic trajectory is computable. A verification (not shown) that this width does indeed recover the stochastic behavior near the hyperbolic trajectory at $t = 5$ was performed by seeding many more particles near the origin in the initial curve of Fig. 3(a).

Figure 4 examines two other initial curves [left panel] and their resulting stochastic advection [right panel]. Generically, the expectation is that all curves would eventually get squashed onto the unstable manifold, and the final uncertainty would be that associated with the unstable manifold. The curves may fold while getting attracted to the unstable manifold, and eventually, characterizing their normal widening becomes meaningless. However, during the transient process, the width expressions are meaningful, as is illustrated by the usage of $R_2(0.5)$ for the two examples in Fig. 4.

Next, the statistics associated with simulations will be compared to the first-order theoretical standard deviation and mean in Eqs. (9) and (7), and the fact that the error is second-order will be verified. The point (0.5,0.5) is fixed as the initial condition $\boldsymbol{x}_{t_1} = \boldsymbol{x}_0$ (i.e., $t_1 = 0$). The curve $\mathcal{C}(t_1)$ will be a curve passing through this point with local slope 1. The idea is to numerically compute N_t as given in Eq. (6) at time $t = 1$, where the s subscript is unnecessary because only one point on the curve is being considered. For computing the local normal and tangent vector, the two points $\boldsymbol{x}_0^{\pm} = \boldsymbol{x}_0 \pm (\delta/\sqrt{2})(1\ 1)^{\top}$, where δ is small (here taken to be fixed at 0.001) are evolved along with $\boldsymbol{x}_t$. The statistics of N_1 from 10^4 simulations is shown in Fig. 5(a), in which $\varepsilon = 0.03$ was used, and $f(N_1)$ is the density of the distribution. The red circles are the frequencies obtained from the Monte Carlo simulations of the 10^4 points, and the red dashed curve is the normal distribution imputed by using the mean and standard deviation of the simulations. It appears that the distribution is, in fact, approximately normal. The solid blue curve is a normal distribution computed using the theoretical mean

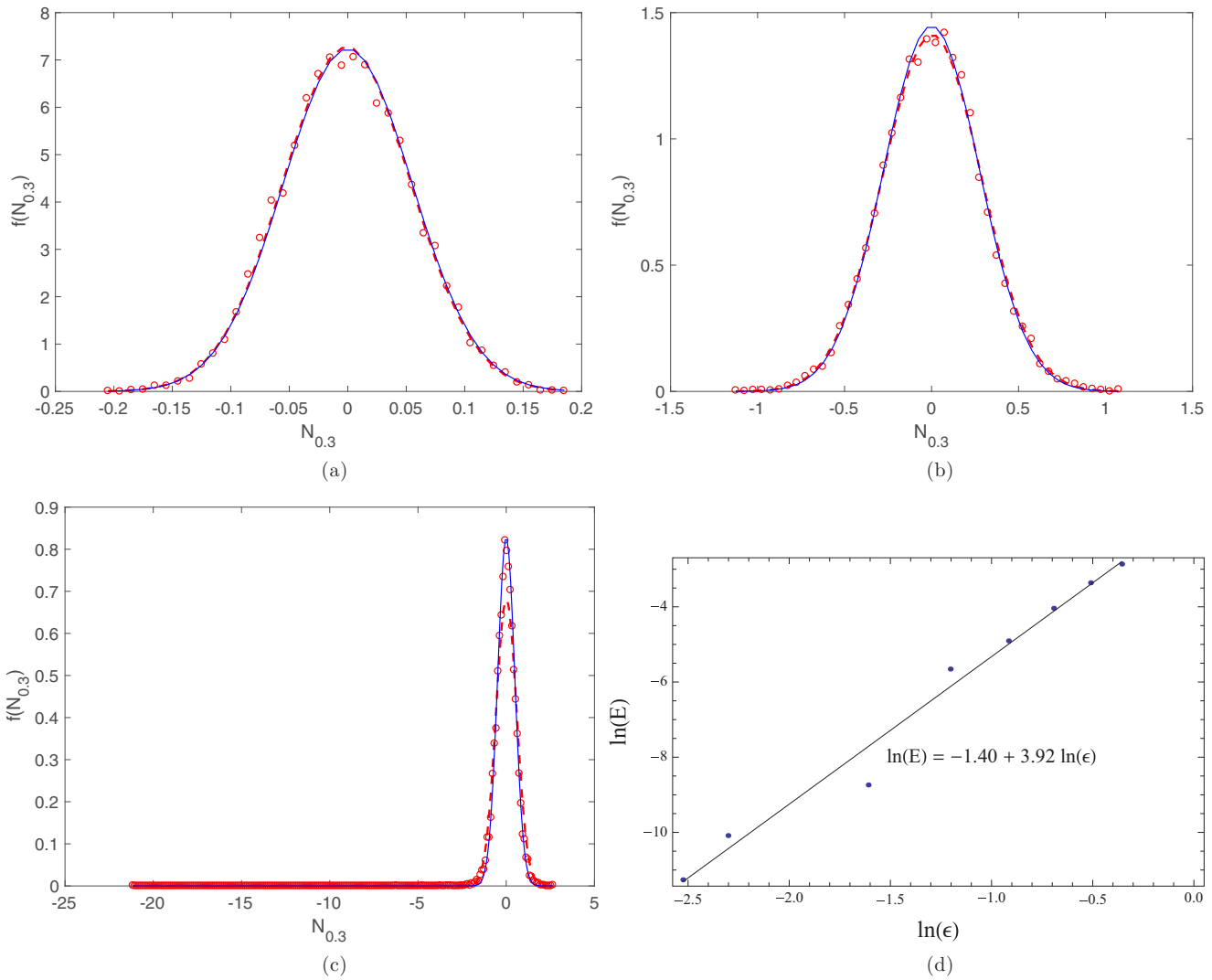

FIG. 7. A comparison of the frequency statistics $f(N_{0.3})$ (red circles), its imputed normal distribution (dashed red curve), and theoretical (normalized) distribution (solid blue curve) for (a) $\varepsilon = 0.08$, (b) $\varepsilon = 0.4$, and (c) $\varepsilon = 0.7$ for the compressible flow as described in the text. (d) Variation of the error Eq. (16) (with subscript 0.3) with ε (blue dots) and a linear fit.

of 0 (from Eq. (7)) and standard deviation (from Eq. (9)). Figures 5(b) and 5(c) show similar simulations at larger ε, with all other parameters kept constant. The agreement between the numerical simulations and the $O(\varepsilon)$ theory clearly worsens as ε increases. To analyze the ε-dependence, define the error function

$$E = |\sqrt{\mathrm{Var}(N_1)} - w_1|, \tag{16}$$

where the variance of N_1 is numerically computed from the 10^4 simulations, and w_1 from the $O(\varepsilon)$ expression, Eq. (9). Figure 5(d) compares $\ln E$ with $\ln \varepsilon$. The computed slope of the log-log plot indicates that the error goes as $O(\varepsilon^{2.29})$, validating the fact that Eq. (9) was claimed to be correct to $O(\varepsilon^2)$. It should be noted that if ε is pushed to smaller numbers, it will be necessary to make δ smaller, to ensure that the errors associated with the normal vector computation are of much smaller size than the standard deviation; here, the fixed value of 0.001 chosen satisfied this over the range of ε considered. Several other simulations with different choices of $\boldsymbol{x}_0$ and local orientations of the curve going through $\boldsymbol{x}_0$ were performed (not shown) and yielded similar results.

V. A COMPRESSIBLE FLOW

This example is to specifically elucidate the role of the compressibility of the flow. To remove deterministic temporal effects, consider

$$\begin{aligned} \dot{x}_1 &= x_1^3 \\ \dot{x}_2 &= 2x_2^2, \end{aligned} \tag{17}$$

and let $\sigma = \mathrm{Id}$ (constant isotropic diffusion) initially. In this case, $\nabla \cdot \boldsymbol{u} = 3x_1^2 + 4x_2$, which is positive when $x_2 > -(3/4)x_1^2$. Since areas chosen within this region expand under the flow Eq. (17), the expectation is that the stochastic width would be larger in this region, and indeed smaller in the region $x_2 < -(3/4)x_1^2$ in which areas compress. The theoretical estimate Eq. (9) incorporates this information in the $\nabla \cdot \boldsymbol{u}$ term in the interior integral, and the idea here is to verify

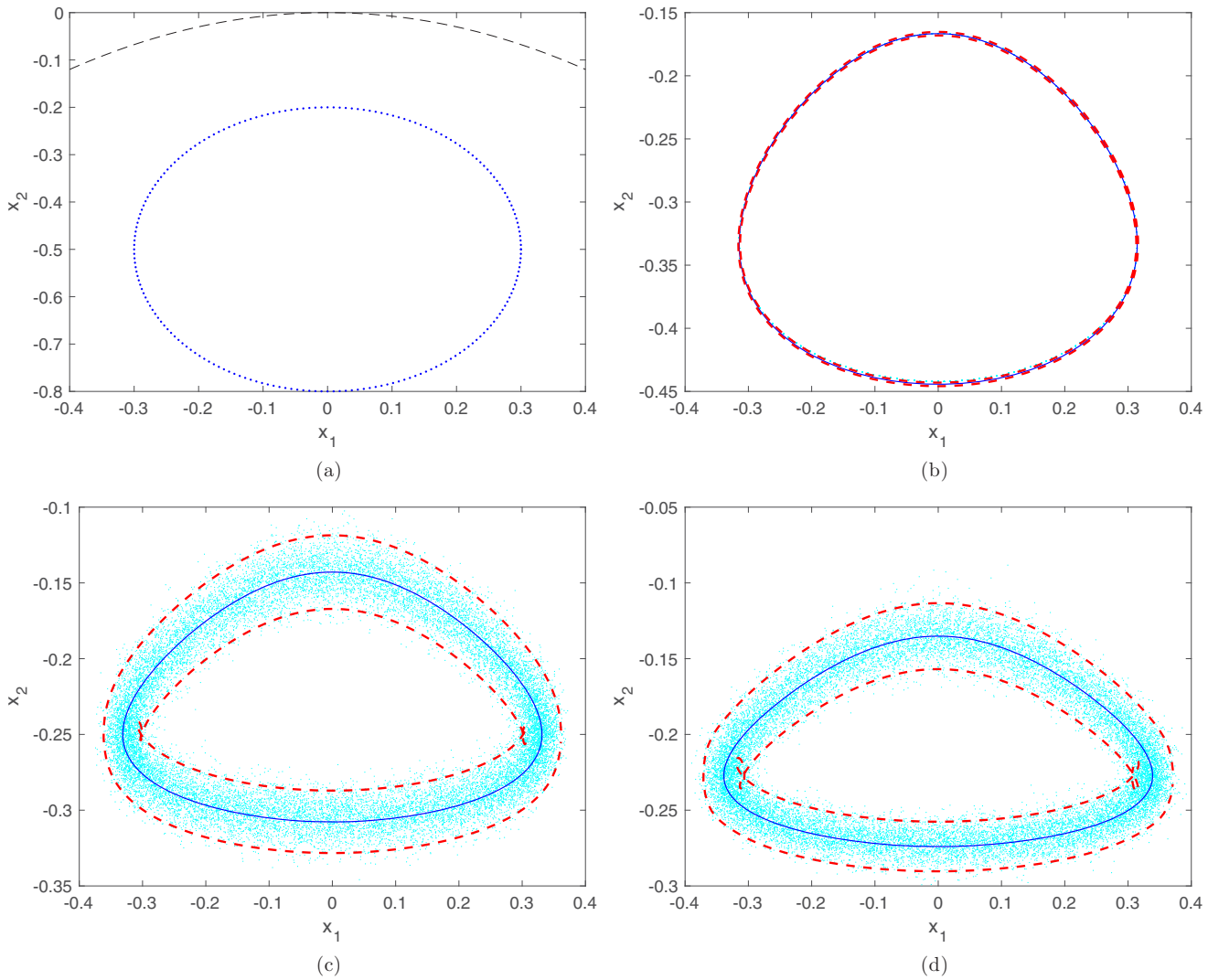

FIG. 8. Original curve (a), and subsequent advected curve points (cyan), with the deterministically advected curve (solid blue) and the theoretical region $R_2(t)$ (dashed red), for the flow Eq. (17) stochastically perturbed with $\sigma(\boldsymbol{x},t) = \chi_{[0.5,1]}(t)\,\mathrm{Id}$: (b) $t = 0.5$, (c) $t = 1$, and (d) $t = 1.2$.

that this captures the combined effects of compressibility and stochasticity.

Figure 6 shows the result of advecting an initial line, shown in Fig. 6(a), by the corresponding stochastic differential equation, in which $\varepsilon = 0.02$. The Euler-Maruyama algorithm uses $\Delta t = 0.01$, to retain the fact that the stochasticity is considered small (i.e., $\varepsilon \ll \Delta t$). Given the facts that the accuracy of the algorithm is $O(\Delta t)$, and the flow Eq. (17) has rapid expansion in x_2 when $x_2 > 0$, numerics can only be computed for relatively short time periods for this choice of parameters. The quantity $\nabla \cdot \boldsymbol{u} > 0$ above the dashed curve $x_2 = -(3/4)x_1^2$ shown in all the figures. As expected, the stochastic trajectories that are within this region for a longer time experience more dispersion, whereas those below the curve [i.e., in the region in which Eq. (17) is compressing] are more tightly situated around the blue curve of deterministic advection. The region $R_2(t)$ is shown by the red dashed curves and is seen to capture the behavior well.

The next task is to quantitatively verify the standard deviation and order of the error. The same initial point, local tangent, and number of simulations (10^4) as for the analogous investigation for the Duffing equation were used. However, here the calculations were done until a final time of 0.3 using $\Delta t = 0.001$, and consequently, $N_{0.3}$ is the random variable whose statistics were analyzed. Figures 7(a)–7(c) show the frequency statistics generated at different ε values, using the same notation as for Fig. 5. There is asymmetry at the largest value of ε pictured, with a long (but thin) tail extending in the negative $N_{0.3}$ direction. However, the distribution appears to approach normality for smaller ε. Figure 7(d) shows the ε-dependence of the error E [as defined in Eq. (16) but with the subscript 0.3] in the standard deviation, and in this case it appears that the error is $\sim O(\varepsilon^4)$, amply justifying the claim that Eq. (9) was correct to $O(\varepsilon^2)$. The higher accuracy may be because the deterministic flow is regular (unlike in the Duffing example) in spite of being compressible.

Finally, the impact of time-variation in σ is considered, by taking $\sigma(x,t) = \chi_{[0.5,1]}(t)\,\mathrm{Id}$, where χ is the indicator function. This means that the stochasticity is only operating for $t \in [0.5,1]$. The stochastic advection is now performed

with the circle as shown in Fig. 8(a) as the initial curve. Here, the calculations can be performed for a longer time than the previous ones, since this lies in $x_2 < 0$ [the line $x_1 = 0$ is invariant for Eq. (17), and so this curve cannot venture into the region $x_2 > 0$ to experience substantial expansion in x_2], and is also within the compressing region for some time. There is no uncertainty at $t = 0.5$, since the stochasticity only kicks in at this point. The (red-dashed) region boundary curves fall exactly on the (blue) deterministic curve in this instance. By $t = 1$, stochastic trajectories have dispersed around the curve, and by $t = 1.2$, this dispersion persists, although there is no accumulated dispersion from the motion for $t \in [1,1.2]$ because the stochasticity has been switched off. Once again, the theoretical region $R_2(t)$ shown in red does well at elucidating this behavior (though by $t = 1.2$, the advected curve is acquiring sufficient bending at the left- and right-most points to render the width expressions less useful).

VI. CONCLUDING REMARKS

This article has established a method for characterizing the impact of stochasticity on curves advected by an unsteady determinstic two-dimensional flow over a finite time. Specifically, the focus was on how the random curves "widen" from the deterministic curve, and the expectation and variance of this widening was obtained to leading order. The theory allows for the deterministic flow to be compressible, and for the stochastic perturbation to be driven by a Wiener process with spatiotemporally varying diffusion. The width expressions were verified for several examples, by comparing with numerical simulations of the relevant stochastic differential equation using the Euler-Maruyama scheme, and excellent agreement was obtained.

The methodology here is a first step in the pursuit for understanding how stochasticity impacts large scale emergent flow structures in unsteady flows—a topic recently flagged for its importance [26]. In the purely determinstic case, there are a range of methods (falling under the umbrella of Lagrangian coherent structures [2–4]), which try to find flow structures which are pertinent to transport. One future application of the current method would be to analyze the robustness to stochasticity of curves which emerge as important transport entities. Such a curve could, for example, be a stable or unstable manifold [3], the outermost curve which demarcates a Lagrangian eddy [27], a strong ridge curve of a finite-time Lyapunov exponent field [2,28], a curve expressing a sharp gradient of a relevant observable such as sea-surface temperature [10], etc. Many of these are usually obtained from numerical simulations of a deterministic velocity field, and therefore the methods of this article allow for characterizing the stochastic uncertainty of such entities. A concurrent study [29] on quantifying the stochastic uncertainty of stable and unstable manifolds is underway.

Another direction in which the present approach offers promise is in the potential for determining the stochastic susceptibility for entities *other than curves* (for example, regions such as the interior of an eddy). This might be accomplished by examining general points in space and developing a theory for the widening at each such point in relation to *all* local curves passing through it (the statistical analyses of Figs. 5 and 7 examined only *one* such curve). This could establish the notion of the stochastic susceptibility of each point in space, and promising steps have been made in this direction (to be reported in a future paper). In these approaches, the fundamental issue that is being addressed is the *interaction* between structures associated with the deterministic dynamics and stochasticity. Are there particular aspects of deterministic structures that can be identifiable as being *more* susceptible to stochasticity? Are there structures that are particularly robust? Pursuing these and allied ideas will lead to a better understanding of the impact of stochasticity (or under-resolved or unmodeled effects) on transport and coherent structures in unsteady flows.

ACKNOWLEDGMENTS

The Australian Research Council supported this Research via Future Fellowship Grant No. FT130100484. Support from the Banff International Research Station for the workshop on "Transport in Unsteady Flows: from Deterministic Structures to Stochastic Models and Back Again" helped inspire this article. Conversations with Georg Gottwald and insightful comments from two referees, which led to a substantial improvements, are gratefully acknowledged.

APPENDIX A: PROOF OF RANDOM NORMAL DISPLACEMENT EQUATION (6)

Fix $t \in [t_1,t_2]$, and let $\xi \in [t_1,t]$ be the temporal variable expressing the evolution from time t_1 to t. Since $\boldsymbol{x}_\xi^s$ is a solution to Eq. (2),

$$\frac{\partial \boldsymbol{x}_\xi^s}{\partial \xi} = \boldsymbol{u}\big(\boldsymbol{x}_\xi^s,\xi\big).$$

Differentiating with respect to s leads to

$$\frac{\partial}{\partial \xi}\left(\frac{\partial \boldsymbol{x}_\xi^s}{\partial s}\right) = \nabla \boldsymbol{u}\big(\boldsymbol{x}_\xi^s,\xi\big)\,\frac{\partial \boldsymbol{x}_\xi^s}{\partial s},$$

which states that $\partial \boldsymbol{x}_\xi^s/\partial s$ is a solution to the equation of variations of Eq. (2). Henceforth in this proof, s shall be fixed, and the notation

$$\boldsymbol{x}_\xi := \boldsymbol{x}_\xi^s, \quad \boldsymbol{y}_\xi := \boldsymbol{y}_\xi^s, \quad \text{and} \quad \boldsymbol{S}_\xi := \frac{\partial \boldsymbol{x}_\xi^s}{\partial s}$$

will be adopted (i.e., the superscript s will be dropped). Thus,

$$\dot{\boldsymbol{x}}_\xi = \boldsymbol{u}(\boldsymbol{x}_\xi,\xi) \quad \text{and} \quad \dot{\boldsymbol{S}}_\xi = \nabla \boldsymbol{u}(\boldsymbol{x}_\xi,\xi)\,\boldsymbol{S}_\xi. \tag{A1}$$

Next, define the Itô process

$$M_\xi(\boldsymbol{y}_\xi) := (\boldsymbol{y}_\xi - \boldsymbol{x}_\xi)\cdot \boldsymbol{S}_\xi^\perp = (\boldsymbol{y}_\xi - \boldsymbol{x}_\xi)^\top \boldsymbol{S}_\xi^\perp \tag{A2}$$

for solutions $\boldsymbol{y}_\xi$ to the stochastic differential Eq. (3). Upon defining

$$J := \begin{pmatrix} 0 & -1 \\ 1 & 0 \end{pmatrix},$$

it is clear that the operation $\perp$ is equivalent to premultiplication by J. Thus,

$$M_\xi(\boldsymbol{y}_\xi) = (\boldsymbol{y}_\xi - \boldsymbol{x}_\xi)^\top J\,\boldsymbol{S}_\xi \tag{A3}$$

and moreover from Eq. (4),

$$M_\xi(\boldsymbol{y}_\xi) = N^s_\xi \left| \frac{\partial \boldsymbol{x}^s_\xi}{\partial s} \right| = N^s_\xi |\boldsymbol{S}_\xi|, \quad \xi \in [t_1, t]. \tag{A4}$$

Itô's lemma [16,17] applied to the Itô process Eq. (A3) now states that

$$dM_\xi = \left[\frac{\partial M_\xi}{\partial \xi} + (\nabla M_\xi)^\top \boldsymbol{u} + \frac{1}{2} \mathrm{Tr}\{(\varepsilon\sigma)^\top (\nabla\nabla M_\xi)(\varepsilon\sigma)\} \right] d\xi + (\nabla M_\xi)^\top (\varepsilon\sigma) d\boldsymbol{W}_\xi,$$

where ∇M_ξ represents the derivative of M_ξ with respect to its $\boldsymbol{y}_\xi$ argument, and $\nabla\nabla M_\xi$ is the Hessian with respect to $\boldsymbol{y}_\xi$. Fortunately, M_ξ is linear in $\boldsymbol{y}$, and the Hessian contains only zero entries. This allows the expression

$$dM_\xi = \left[\frac{\partial M_\xi}{\partial \xi} + (\nabla M_\xi)^\top \boldsymbol{u} \right] d\xi + (\nabla M_\xi)^\top (\varepsilon\sigma) d\boldsymbol{W}_\xi,$$

where the spatial argument of every term is $\boldsymbol{y}_\xi$ and the temporal argument is ξ. Taking the appropriate derivatives of Eq. (A3) yields

$$\begin{aligned} dM_\xi &= [(\boldsymbol{y} - \boldsymbol{x}_\xi)^\top J \dot{\boldsymbol{S}}_\xi - \dot{\boldsymbol{x}}_\xi^\top J \boldsymbol{S}_\xi + (J\boldsymbol{S}_\xi)^\top \boldsymbol{u}] d\xi \\ &\quad + \varepsilon (J\boldsymbol{S}_\xi)^\top \sigma d\boldsymbol{W}_\xi \\ &= [(\boldsymbol{y} - \boldsymbol{x}_\xi)^\top J \nabla \boldsymbol{u}(\boldsymbol{x}_\xi, \xi) \boldsymbol{S}_\xi - \boldsymbol{u}(\boldsymbol{x}_\xi, \xi)^\top J \boldsymbol{S}_\xi \\ &\quad + (J\boldsymbol{S}_\xi)^\top \boldsymbol{u}(\boldsymbol{y}, \xi)] d\xi + \varepsilon (J\boldsymbol{S}_\xi)^\top \sigma(\boldsymbol{y}, \xi) d\boldsymbol{W}_\xi \\ &= [(\boldsymbol{y} - \boldsymbol{x}_\xi)^\top J \nabla \boldsymbol{u}(\boldsymbol{x}_\xi, \xi) \boldsymbol{S}_\xi - \boldsymbol{u}(\boldsymbol{x}_\xi, \xi)^\top J \boldsymbol{S}_\xi \\ &\quad + (J\boldsymbol{S}_\xi)^\top \boldsymbol{u}(\boldsymbol{x}_\xi, \xi) + (J\boldsymbol{S}_\xi)^\top \nabla \boldsymbol{u}(\boldsymbol{x}_\xi, \xi)(\boldsymbol{y} - \boldsymbol{x}_\xi)] d\xi \\ &\quad + \varepsilon (J\boldsymbol{S}_\xi)^\top \sigma(\boldsymbol{x}_\xi, \xi) d\boldsymbol{W}_\xi + O(\varepsilon^2), \end{aligned}$$

where Eq. (A1) has been used for the second equality, and a Taylor expansion of $\boldsymbol{u}(\boldsymbol{y}, \xi)$ and $\sigma(\boldsymbol{y}, \xi)$ around $(\boldsymbol{x}_\xi, \xi)$ in the third. Since integration will only be done over a finite-time, $\boldsymbol{y} - \boldsymbol{x}_\xi$ is $O(\varepsilon)$, and hence the next-order terms in the Taylor expansion are $O(\varepsilon^2)$ as long as the second-order spatial derivatives of $\boldsymbol{u}$ and the first-order spatial derivative of σ are bounded in $\Omega \times [t_1, t_2]$. The second and third terms—each being the dot product between $\boldsymbol{u}$ and $J\boldsymbol{S}_\xi$—cancel. Next, the identity

$$\boldsymbol{b}^\top J A \boldsymbol{c} + (J\boldsymbol{c})^\top A \boldsymbol{b} = (\mathrm{Tr}\, A) \boldsymbol{b}^\top J \boldsymbol{c} \tag{A5}$$

for 2×1 vectors $\boldsymbol{b}$ and $\boldsymbol{c}$, and any 2×2 matrix A, is asserted [30]. Setting $A = \nabla \boldsymbol{u}$, $\boldsymbol{b} = \boldsymbol{y} - \boldsymbol{x}_\xi$ and $\boldsymbol{c} = \boldsymbol{S}_\xi$, and realizing that $\mathrm{Tr}\,(\nabla \boldsymbol{u}) = \nabla \cdot \boldsymbol{u}$ leads to

$$\begin{aligned} dM_\xi &= [(\nabla \cdot \boldsymbol{u})(\boldsymbol{y} - \boldsymbol{x}_\xi)^\top J \boldsymbol{S}_\xi] d\xi \\ &\quad + \varepsilon (J\boldsymbol{S}_\xi)^\top \sigma \, d\boldsymbol{W}_\xi + O(\varepsilon^2) \\ &= [(\nabla \cdot \boldsymbol{u}) M_\xi] d\xi + \varepsilon (J\boldsymbol{S}_\xi)^\top \sigma \, d\boldsymbol{W}_\xi + O(\varepsilon^2), \end{aligned}$$

where $\boldsymbol{u}$ and σ are both evaluated at the spatio-temporal values $(\boldsymbol{x}_\xi, \xi)$. Using the standard integrating-factor approach permits the rewriting

$$\begin{aligned} &d\left[e^{-\int_{t_1}^{\xi} [\nabla \cdot \boldsymbol{u}](\boldsymbol{x}_\eta, \eta) d\eta} M_\xi \right] \\ &\quad = \varepsilon e^{-\int_{t_1}^{\xi} [\nabla \cdot \boldsymbol{u}](\boldsymbol{x}_\eta, \eta) d\eta} (J\boldsymbol{S}_\xi)^\top \sigma(\boldsymbol{x}_\eta, \xi) d\boldsymbol{W}_\xi + O(\varepsilon^2). \end{aligned}$$

Now, since at time t_1 the curves $\mathcal{C}$ and $\mathfrak{C}$ coincide, $N^s_{t_1} = 0$ for any s. Therefore, from Eq. (A4), $M_{t_1}(\boldsymbol{y}_{t_1}) = 0$. The integral formulation of the above at a general time t then becomes

$$M_t(\boldsymbol{y}_t) = \varepsilon \int_{t_1}^{t} e^{\int_\xi^t [\nabla \cdot \boldsymbol{u}](\boldsymbol{x}_\eta, \eta) d\eta} (J\boldsymbol{S}_\xi)^\top \sigma(\boldsymbol{x}_\xi, \xi) d\boldsymbol{W}_\xi + O(\varepsilon^2), \tag{A6}$$

where the error remains $O(\varepsilon^2)$ since the integration is over a finite time interval. Finally, applying the connection Eq. (A4) between M_t and N^s_t and reverting to the original notation gives the result Eq. (6), in which the $O(\varepsilon^2)$ terms have been omitted.

APPENDIX B: CLARIFICATIONS TO EQUATIONS (6) AND (9)

First, a very rough estimate is made of the time-interval in which using Eq. (9), the $O(\varepsilon)$ part of the full expression, could be deemed legitimate. Going through the derivation in Appendix A, it is clear that when expressing $d\boldsymbol{M}_\xi$, the $O(\varepsilon^2)$ terms include both $d\xi$ and $d\boldsymbol{W}_\xi$ terms. Thus, when integrated, this would result in bounds of the form $C_1(t - t_1)$ and $C_2\sqrt{t - t_1}$ for constant C_i. In investigating the largest time validity, the larger of these needs to be taken. Now, it is exactly this term that gets carried over to the determination of $\boldsymbol{w}^s_t$, and thus for the $O(\varepsilon)$ term of $\boldsymbol{w}^s_t$ as given in Eq. (9) to be of greater relevance than the next-order term, the requirement is

$$\frac{\varepsilon \left(\int_{t_1}^{t} e^{2\int_\xi^t [\nabla \cdot \boldsymbol{u}](\boldsymbol{x}^s_\eta, \eta) d\eta} \left| \sigma^\top \left(\boldsymbol{x}^s_\xi, \xi \right) \left(\frac{\partial \boldsymbol{x}^s_\xi}{\partial s} \right)^\perp \right|^2 d\xi \right)^{1/2}}{\left| \frac{\partial \boldsymbol{x}^s_t}{\partial s} \right|} \gg C_1 \varepsilon^2 (t - t_1).$$

Estimating the terms on the left with some constant bound C_2 yields

$$C_2 \varepsilon \sqrt{t - t_1} \gg C_1 \varepsilon^2 (t - t_1) \Rightarrow \sqrt{t - t_1} \ll C \frac{1}{\varepsilon},$$

which indicates that the time-validity of the first-order Eq. (9) goes as $t - t_1 \sim \varepsilon^{-2}$. However, there is a caveat to this: Eq. (9) also loses validity if the deterministic curve folds unduly, because in that case the normal vector $\hat{\boldsymbol{n}}^s_t$ changes too rapidly with s for $\cup_s [\boldsymbol{x}^s_t \pm \varepsilon \alpha w^s_t \hat{\boldsymbol{n}}^s_t]$ to meaningfully define a curve widening.

Next, simplifications to the random width Eq. (6) and its standard derivation Eq. (9) are addressed.

(1) If the fluid is incompressible, $\nabla \cdot \boldsymbol{u} = 0$, and thus

$$N^s_t = \frac{\varepsilon \int_{t_1}^{t} \left(\left[\frac{\partial \boldsymbol{x}^s_\xi}{\partial s} \right]^\perp \right)^\top \sigma \left(\boldsymbol{x}^s_\xi, \xi \right) d\boldsymbol{W}_\xi}{\left| \frac{\partial \boldsymbol{x}^s_t}{\partial s} \right|} \tag{B1}$$

and

$$w^s_t = \frac{\varepsilon \left(\int_{t_1}^{t} \left| \sigma^\top \left(\boldsymbol{x}^s_\xi, \xi \right) \left(\frac{\partial \boldsymbol{x}^s_\xi}{\partial s} \right)^\perp \right|^2 d\xi \right)^{1/2}}{\left| \frac{\partial \boldsymbol{x}^s_t}{\partial s} \right|}. \tag{B2}$$

(2) If the Wiener process is derived from a Brownian motion, which is not modulated by any spatial or temporal dependence, and with the Brownian motions in the two coordinate directions uncorrelated, then $\sigma = \mathrm{Id}$ (the identity). This can be thought of as the situation of constant and isotropic

diffusion. Then,

$$N_t^s = \frac{\varepsilon \int_{t_1}^{t} e^{\int_\xi^t [\nabla\cdot\boldsymbol{u}](\boldsymbol{x}_\eta^s,\eta)d\eta} \left(\frac{\partial \boldsymbol{x}_\xi^s}{\partial s}\right)^\perp \cdot d\boldsymbol{W}_\xi}{\left|\frac{\partial \boldsymbol{x}_t^s}{\partial s}\right|}, \tag{B3}$$

and moreover the $\perp$ sign can be deleted from the w expression, resulting in

$$w_t^s = \frac{\varepsilon\left(\int_{t_1}^{t} e^{2\int_\xi^t [\nabla\cdot\boldsymbol{u}](\boldsymbol{x}_\eta^s,\eta)d\eta} \left|\frac{\partial \boldsymbol{x}_\xi^s}{\partial s}\right|^2 d\xi\right)^{1/2}}{\left|\frac{\partial \boldsymbol{x}_t^s}{\partial s}\right|}. \tag{B4}$$

(3) If the fluid is incompressible *and* the diffusion is isotropic, then

$$N_t^s = \frac{\varepsilon}{\left|\frac{\partial x}{\partial s}(s,t)\right|} \int_{t_1}^{t} \left(\frac{\partial \boldsymbol{x}_\xi^s}{\partial s}\right)^\perp \cdot d\boldsymbol{W}_\xi, \tag{B5}$$

$$w_t^s = \varepsilon\left(\int_{t_1}^{t} \left(\left|\frac{\partial \boldsymbol{x}_\xi^s}{\partial s}\right| \Big/ \left|\frac{\partial \boldsymbol{x}_t^s}{\partial s}\right|\right)^2 d\xi\right)^{1/2}. \tag{B6}$$

It is this last expression that is rewritten in Eq. (11). It should also be borne in mind that in all the expressions given for N_t^s and w_t^s in this Appendix, there should be an additive $O(\varepsilon^2)$ term, which has been omitted for brevity.

[1] T. Peacock and J. Dabiri, Chaos **20**, 017501 (2010).
[2] G. Haller, Annu. Rev. Fluid Mech. **47**, 137 (2015).
[3] S. Balasuriya, *Barriers and Transport in Unsteady Flows: A Melnikov Approach*, Mathematical Modeling and Computation (SIAM Press, Philadelphia, 2016).
[4] S. Shadden, in *Transport and Mixing in Laminar Flows: From Microfluidics to Oceanic Currents*, edited by R. Grigoriev (Wiley, New York, 2011).
[5] A. E. BozorgMagham and S. D. Ross, Commun. Nonlin. Sci. Numer. Simu. **22**, 964 (2015).
[6] A. M. Thurnherr, J. Atmos. Oceanic Tech. **27**, 1215 (2010).
[7] P. S. Berloff and J. C. McWilliams, J. Phys. Oceanogr. **32**, 797 (2002).
[8] R. H. Kraichnan, Phys. Fluids **11**, 945 (1968).
[9] M. Vlad and F. Spineanu, Phys. Rev. E **70**, 056304 (2004).
[10] J. H. LaCasce, Progr. Oceanogr. **77**, 1 (2008).
[11] P. H. Roberts, J. Fluid Mech. **11**, 257 (1961).
[12] R. H. Kraichnan, Phys. Fluids **13**, 22 (1970).
[13] A. Careta, F. Sagués, L. Ramírez-Piscina, and J. Sancho, J. Stat. Phys. **71**, 235 (1993).
[14] J. Vanneste, J. Atmos. Sci. **61**, 2749 (2004).
[15] S. V. Azarina and Y. E. Gliklikh, Math. Notes **100**, 3 (2016).
[16] B. Oksendal, *Stochastic Differential Equations* (Springer, Berlin, 1995).
[17] G. Kallianpur and P. Sundar, *Stochastic Analysis and Diffusion Processes*, Graduate Texts in Mathematics (Oxford Universiry Press, Oxford, 2014).
[18] J. D. Wilson and B. L. Sawford, Boundary-Layer Meteor. **78**, 191 (1996).
[19] S. Balasuriya, SIAM J. Appl. Dyn. Sys. **10**, 1100 (2011).
[20] There is no claim, however, that this is rigorously correct, since the nature of the distribution of N_t^s in Eq. (6) is not known precisely, apart from its expectation and variance. Generally, non-Gaussian statistics are to be expected [31].
[21] G. I. Taylor, Proc. Lond. Math. Soc. **s2-20**, 196 (1922).
[22] D. Elhmaïdi, A. Provenzale, and A. Babiano, J. Fluid Mech. **257**, 533 (1993).
[23] C. Van den Broeck, Physica A **168**, 677 (1990).
[24] J. Guckenheimer and P. Holmes, *Nonlinear Oscillations, Dynamical Systems, and Bifurcations of Vector Fields* (Springer, New York, 1883).
[25] P. Kloeden and E. Platen, *Numerical Solution of Stochastic Differential Equations* (Springer, Berlin, 1992).
[26] S. Balasuriya, D. Crommelin, G. Froyland, A. Monahan, N. Ouellette, and L. Zanna, Transport in Unsteady Flows: From Deterministic Structures to Stochastic Models and Back Again, Tech. Rep. (Banff International Research Station Workshop Reports, January 15–20, 2017).
[27] G. Haller, A. Hadjighasem, M. Farazmand, and F. Huhn, J. Fluid Mech. **795**, 136 (2016).
[28] S. Balasuriya, R. Kalampattel, and N. T. Ouellette, J. Fluid Mech. **807**, 509 (2016).
[29] S. Balasuriya and G. Gottwald (unpublished).
[30] This is a standard identity available elsewhere in many forms; see Eq. (2.39) in Ref. [3], Eq. (4.5.8) in Ref. [24], or Section 3.1 in Ref. [19].
[31] W. Tang and A. Mahalov, Phys. Plasmas **20**, 032305 (2013).